PENERBIT UMP PRESS

ORIGINAL ARTICLE

The Effect of Welding Parameter on Mechanical Properties and Macrostructure of AA1100 using Autogenous TIG Welding

Ario Sunar Baskoro*, Indra Milyardi and Mohammad Azwar Amat

Mechanical Engineering Department, Faculty of Engineering, Universitas Indonesia, Depok INDONESIA
Phone: +62-21-7270032; Fax: +62-21-7270033

ABSTRACT – In this paper, an autogenous tungsten inert gas (TIG) welding was performed to understand the characteristic effect of butt joint weld on AA1100 under various parameters. The effect of TIG current and welding speed was selected to study the mechanical properties, porosity, and macrostructure of the weld metal (WM). Based on experimental results, the top bead width (TBW) will increase directly proportional to the increased of welding current. Furthermore, welding current and welding speed affected the strength drop in the heat-affected zone (HAZ). More heat added will result in a deeper drop in strength. Mechanical properties result showed that the tensile strength reduced by 40 – 45% and the hardness reduction in the WM and HAZ area from the base metal (BM) was 17.3% and 27.7%, respectively. Subsequently, x-ray radiography images showed that there was no large porosity occur in all welding current. The macrostructure showed that the weld bead typically has the concavity shape or U-shaped geometry from a cross-sectional view.

INTRODUCTION

Aluminium alloys have become the most widely used material in industries and become an integral part of the aerospace and transportation industry [1]. Aluminium alloys have many advantages, such as excellent mechanical properties, low density, good formability, recyclability, and highly corrosion resistance. There are many ways to join aluminium alloys such as fusion welding (TIG/MIG), friction stir welding (FSW) [2], torch brazing [3], resistance spot welding [4], laser beam welding [5], and others. However, joining aluminium alloys is a problematic part. Aluminium alloys do not have good weldability, especially using fusion welding. The presence of a tenacious oxide layer, the high solubility of hydrogen, high coefficient of thermal expansion, and high thermal conductivity are the disadvantages of aluminium alloys properties [6].

Joining aluminium alloys using fusion welding can lead to the welding defect, such as porosity, solidification cracking, undercut, incomplete fusion, and spatter [7]. Moreover, the reduction of mechanical strength and alteration of microstructure are the problem that needs to be solved. On the other hand, joining using fusion welding generally, are more economical and flexible compared to the FSW [8]. The necessity to understand how aluminium alloys behave when they are joining together is a crucial part, and an essential need in many industries used aluminium as main or sub material. Furthermore, finding the optimal parameters to reduce the susceptibility of solidification cracking, lowering the potential of welding porosity, and decreasing the reduction of the welding joint strength coefficient can be challenging.

Gas tungsten arc welding (GTAW), also known as Tungsten Inert Gas (TIG) welding is a fusion welding process in which an electric arc is created in an inert gas such as helium (He) or argon (Ar) between non-consumable tungsten and workpiece [9]. GTAW can be used to weld butt joint using the addition of filler metals or without filler metals (also known as Autogenous welding) [10]. Some researchers investigated the effect of different filler metals to join similar aluminium alloys [11] and super-austenitic steel [12]. On the other hand, researchers have performed dissimilar joint material such as aluminium to galvanized steel [13] and aluminium to stainless steel [14]. The other focused on controlling TIG welding using machine vision and neural network [15]. Most of the researchers investigated the mechanical properties and microstructure as a critical aspect for evaluation [7, 16]. Several researchers concerned with welding defects such as porosity. Huang et al. [17] investigated the porosity on aluminium alloys using spectral and X-ray image analysis. Li et al. [18] studied the effect of welding parameters on microstructure and porosity.

In the previous research, Milyardi and Baskoro [19] investigated the effect of welding current and welding speed on weld porosity using a non-destructive test (NDT) such as X-ray radiography. The research determined the proper welding current and welding speed to produce minimum porosity. They found that welding current 160 A and welding speed 1.1 mm/s would generate proper heat input to achieve minimum porosity formation. Therefore, the objectives of this study are to determine the proper parameter to weld aluminium alloy AA1100 of 3 mm in thickness using autogenous TIG welding. Moreover, it is to understand how aluminium alloys behave in each parameter by observing the macrostructure, porosity, tensile properties, and micro-hardness.

MATERIALS AND METHOD

The materials used in this study were AA1100-H14 with a thickness of 3 mm. The chemical composition of AA1100 was tested using an optical emission spectrometer (standard ASTM E1251). The chemical composition is shown in Table 1. The mechanical properties of base metal AA1100 were tested. A tensile test and micro-hardness measurement of the base metal are shown in Table 2.

Table 1. Composition of AA1100.

Element	Al	Si	Fe	Cu	Mn	Mg	Zn	Ti
wt.%	99.1	0.109	0.471	0.057	0.043	0.019	0.070	0.012

Table 2. Material properties of AA1100-H14

Properties		
Hardness	(HV)	36 – 38
Ultimate tensile strength	(MPa)	130
Tensile yield strength	(MPa)	110 – 120

Aluminium alloys were cut into 50x120mm^2 using the cutter tools. TIG welding machine used GeKaMac Power TIG 2200 AC/DC pulse. The material surface was treated to eliminate the oxide layer using sandpaper with 400 grit number and cleaned chemically using acetone to remove the oil and small particles. AC polarity was employed in the welding process with a frequency of 250 Hz. During the welding process, the average excitation voltage was between 13-15 volts. At the initial welding process, a delay of 15 seconds was given. High purity argon was used as a shielding gas with a flow rate of 12 L/min at the top side welded pool and 3 L/min at the bottom side weld pool. The tungsten electrode was set perpendicular to the workpiece with a distance of 2 mm. Butt joint configuration with square-groove was employed with no gap, and they were clamped using the fixture to avoid distortion. The welding parameters used in this study were shown in Table 3. Figure 1 shows the schematic illustration of the experimental setup.
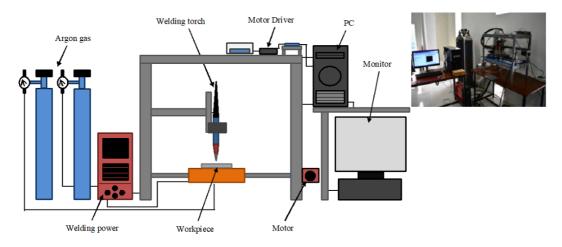

Figure 1. Schematic illustration of experimental equipment.

Table 3. Welding process parameters.

Parameter	Specification
Polarity	AC (250Hz)
Welding current (A)	160-170
Welding speed (mm/s)	1.0-1.2
Electrode	EWTH-2 (Ø 2.4 mm)
Tungsten distance to material (mm)	2
Shielding gas	Pure Argon
Top side shielding gas flow rate (l/min)	12
Bottom side shielding gas flow rate (l/min)	3
Initial welding process time delay (sec)	15

As shown in Figure 2, measurements of the top bead width (TBW) were employed along the welded in 8 locations. Subsequently, X-Ray radiography was performed to detect porosity. Tensile testing was employed using Tensilon RTF-2350, a universal testing machine 50 kN. The crosshead displacement rate was used 5 mm/min. The specimen dimension

was following a standard of ASTM E-8M. Macro and microstructure observation was conducted using DINO-LITE and Oxion Inverso OX.2153-PLM. The specimen was prepared following standard metallography procedure and using etched 0.5% HF solution. Micro-hardness measurement used a load of 100 gf, and 15 sec dwell time, the micro-hardness distribution shows in Figure 3.
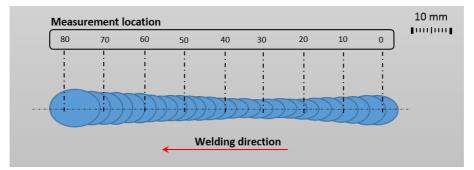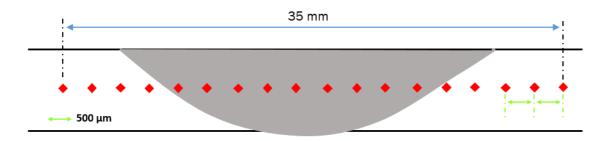

Figure 2. Schematic measurement of TBW.

Figure 3. Schematic illustration of micro-hardness measurement (not for scale).

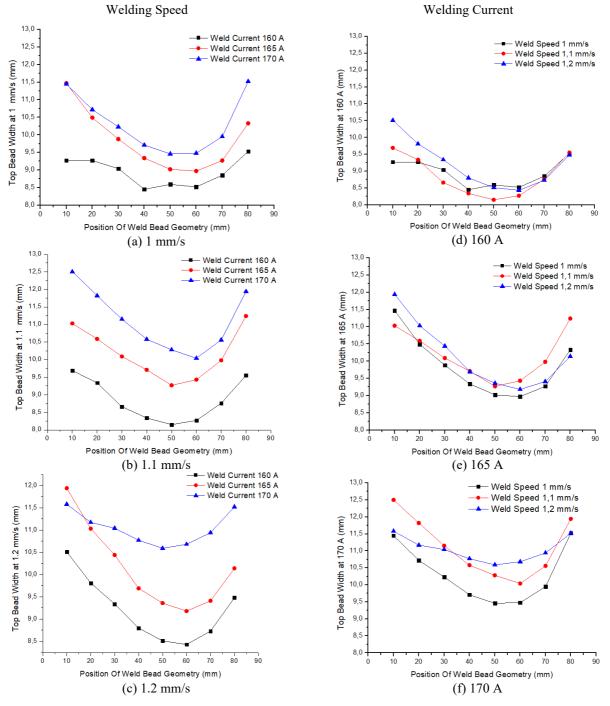## RESULTS AND DISCUSSION

Macrostructures

Figure 4(a) to 4(f) shows the average value of the TBW from 3 samples. The weld bead geometry formed U-shaped geometry in all variations. The largest size weld bead at location number 1 is a result of the time delay at the initial welding, giving more heat input on that spot, hence the weld pool became large. After a while, the weld pool becomes narrower when the heat input was fast enough to disperse into all body (volume) of workpiece and anvil to increase their temperatures until its steady. This is mainly due to the high thermal conductivity of aluminium alloys properties [6]. Afterwards, the weld pool size increasing again as a result of the temperature of the workpiece and anvil on the steady condition. Hence the dispersion becomes slower and more heat to melt the joint.
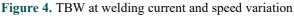
Figure 4(a) to (c) show a result of weld bead width under various welding current in specific welding speed. Figure 4(d-f) show a result of weld bead width under various welding speed in a specific welding current. Figure 4(a-c) show higher welding current produce higher heat input and resulted in the wider weld pool. Theoretically, higher speed will give lower heat input (J/mm) and tend to have a smaller size in the weld pool. However, Figure 4(d) to (f) shows insignificant results. This could be due to the insignificant difference in speed variation. Hence, the results are in the region of standard deviation.
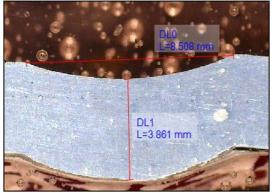
Figure 5(a) to (c) show the cross-sectional macrostructure observation. DL0 is the concavity length, and DL1 is the weld thickness. It is shown that DL0 increases while welding current increases, and DL1 increases in thickness from 3 mm (base metal thickness) to a range of 3.7 – 4.0 mm.
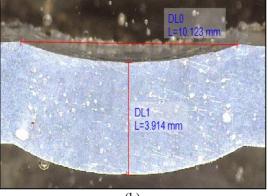
X-Ray Radiography

The X-ray inspection is to detect the porosity distribution across the welded area from the top view of the weldment. Figure 6(a-c) show the porosity appearances at different welding currents. Welding parameters such as welding current have a significant impact on the porosity formation. The results show that increasing the welding current leads to a decrease in porosity formation [19].
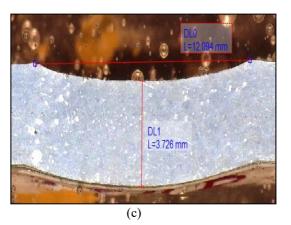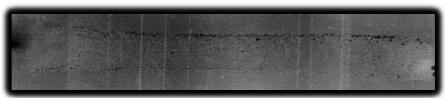
Welding Speed

Welding Current

(a) 1 mm/s

(d) 160 A

(b) 1.1 mm/s

(e) 165 A

(c) 1.2 mm/s

(f) 170 A

Figure 4. TBW at welding current and speed variation

(a)

(b)

(c)

Figure 5. Cross-sectional macrostructure observation of (a) 160 A; (b) 165 A; (c) 170 A.

(a) 160 A

(b) 165 A

(c) 170 A

Figure 6. X-ray images at different welding currents.

Tensile Test

Figure 7 shows the result of tensile test specimens at various welding currents and base metal (BM). Tensile tests are performed to investigate the effect of the welding current on the tensile strength. The strength of the BM is 130 MPa, and the strength at 160 A yields the highest value of 80 MPa compared to 165 A and 170 A, which yield 75.6 MPa and 72 MPa, respectively. It is shown that the reduction of tensile strength is in a range of 40-45% from BM. The strength reduction takes place in the HAZ region, where the annealing occurred. Theoretically, by adding more heat input, more time are required for the material to be exposed to annealing conditions. Therefore, the results are consistent, where 170 A is the lowest, and 160 A is the highest strength and elongation.

Micro-hardness test

Micro-hardness distribution is recorded by performing Vickers indentations on the TIG metallographic sample. Spacing between indentations is 500 µm, and the measurements on the horizontal distribution are carried out approximately 35 mm. Indentations are made on the horizontal distribution across the BM, HAZ, and weld metal (WM). Figure 8 shows the hardness of BM is 37.5±1.0, the hardness of HAZ is 27.1±0.9 HV, and the hardness of WM is 31.0±1.5 HV. It is shown that there is a 17.3% reduction value of hardness with WM compared to the BM, while HAZ shows a reduction value of 27.7% compared to the BM.
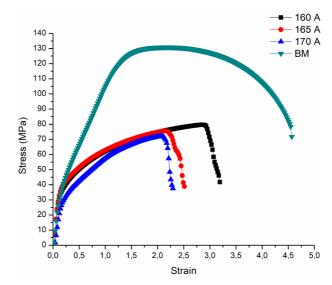
Figure 7. Result of tensile test TIG welding specimens.

Microstructure

Figure 9 shows a typical microstructure of AA1100 using autogenous TIG welding. The typical microstructures can be divided into three visible zones, which are BM, HAZ, and WM. The WM area is composed of dendritic structure mainly found at the centre area, and columnar structure foundnear the fusion line. The HAZ area is where the grains grow and coarse grains are formed. The HAZ region is subjected to a longer temperature between 150°C-250°C. There are micro porosities found in all variations of welding current. By increasing the welding current, porosity can be reduced.
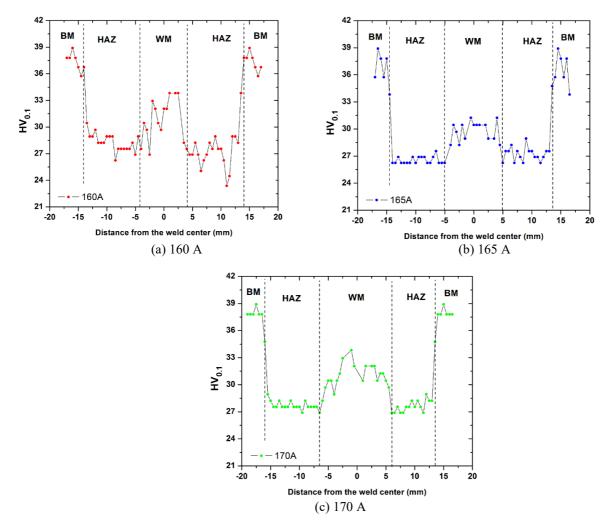

(a) 160 A

(b) 165 A

(c) 170 A

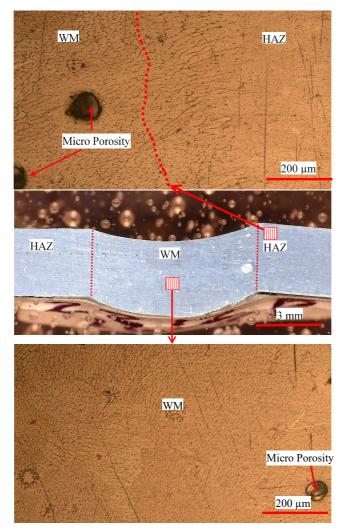**Figure 8.** Micro-hardness profile of TIG welding specimens.

Figure 9. Typical microstructure of weld metal AA1100.

CONCLUSION

The following are conclusions that can be drawn from this investigation:

i.   The width of the weld bead increases as the welding current is increased. The weld bead typically has a concavity shape and forms a U-shaped geometry if observed from a cross-sectional view.

ii.   The reduction of tensile strength is in a range of 40-45% from BM. A smaller welding current have less heat input and allows less time for the HAZ area to be affected by heat, so the anneal effect take a shorter time to form. The resulting drop strength in the HAZ area tends to be smaller compared to the higher welding current (more heat input).

iii. The hardness reduction in the WM and HAZ area compared to the hardness of the BM is 17.3% and 27.7%, respectively.

iv.   Micro-porosity is found in all variations of welding current, and by increasing the welding current, porosity can be reduced.

ACKNOWLEDGEMENT

REFERENCES

[1]   Rajendran C. Evaluation of load-carrying capabilities of friction stir welded, TIG welded and riveted joints of AA2014-T6 aluminum alloy. Aircraft Engineering and Aerospace Technology. 2019; 91(9): 1238-1244.

[2]   Selamat NFM, Baghdadi AH, Sajuri Z, Kokabi AH. Friction stir welding of similar and dissimilar aluminum alloys for automotive applications. International Journal of Automotive and Mechanical Engineering. 2016; 13(2): 3401-3412.

[3]   Baskoro AS, Fauzan A. Effect of pressure and length of lap joint on shear load and joint clearance during dissimilar metal joining using torch brazing for the shipping industry. International Journal of Technology. 2015; 6(4): 604-612.

[4]   Baskoro AS, Muzakki H, Kiswanto G, Winarto. Effects of micro resistance spot welding parameters on the quality of weld joints on aluminum thin plate AA 1100. International Journal of Technology. 2017; 8(7): 1306-1313.

[5]   Bachmann M, Avilov V, Gumenyuk A, Rethmeier M. Numerical assessment and experimental verification of the influence of the Hartmann effect in laser beam welding processes by steady magnetic fields. International Journal of Thermal Sciences. 2016; 101: 24-34.

[6]   Lakshminarayanan AK, Balasubramanian V, Elangovan K. Effect of welding processes on tensile properties of AA6061 aluminum alloy joints. The International Journal of Advanced Manufacturing Technology. 2009; 40(3): 286-296.

[7]   Liang Y, Shen J, Hu S, Wang H, Pang J. Effect of TIG current on microstructural and mechanical properties of 6061-T6 aluminum alloy joints by TIG–CMT hybrid welding. Journal of Materials Processing Technology. 2018; 255: 161-174.

[8]   Hasanniah A, Movahedi M. Welding of Al-Mg aluminum alloy to aluminum clad steel sheet using pulsed gas tungsten arc process. Journal of Manufacturing Processes. 2018; 31: 494-501.

[9]   Mougenot J, Gonzalez JJ, Freton P, Masquère M. Plasma-weld pool interaction in tungsten inert-gas configuration. Journal of Physics D: Applied Physics. 2013; 46(13).

[10] Eisazadeh H, Haines DJ, Torabizadeh M. Effects of gravity on mechanical properties of GTA welded joints. Journal of Materials Processing Technology. 2014; 214(5): 1136-1142.

[11] Ishak M, Noordin NFM, Razali ASK, Shah LHA, Romlay FRM. Effect of filler on weld metal structure of AA6061 aluminum alloy by tungsten inert gas welding. International Journal of Automotive and Mechanical Engineering. 2015; 11(1): 2438-2446.

[12] Devendranath Ramkumar K, Chandrasekhar A, Srivastava A, Preyas H, Chandra S, Dev S, et al. Effects of filler metals on the segregation, mechanical properties and hot corrosion behaviour of pulsed current gas tungsten arc welded super-austenitic stainless steel. Journal of Manufacturing Processes. 2016; 24: 46-61.

[13] Dong H, Hu W, Duan Y, Wang X, Dong C. Dissimilar metal joining of aluminum alloy to galvanized steel with Al-Si, Al-Cu, Al-Si-Cu and Zn-Al filler wires. Journal of Materials Processing Technology. 2012; 212(2): 458-464.

[14] Shah LH, Akhtar Z, Ishak M. Investigation of aluminum-stainless steel dissimilar weld quality using different filler metals. International Journal of Automotive and Mechanical Engineering. 2013; 8(1): 1121-1131.

[15] Baskoro AS, Tandian R, Haikal, Edyanto A, Saragih AS. Automatic Tungsten Inert Gas (TIG) welding using machine vision and neural network on material SS304. 2017: Institute of Electrical and Electronics Engineers Inc.

[16] Vargas JA, Torres JE, Pacheco JA, Hernandez RJ. Analysis of heat input effect on the mechanical properties of Al-6061-T6 alloy weld joints. Materials & Design (1980-2015). 2013; 52: 556-564.

[17] Huang Y, Wu D, Lv N, Chen H, Chen S. Investigation of porosity in pulsed GTAW of aluminum alloys based on spectral and X-ray image analyses. Journal of Materials Processing Technology. 2017; 243: 365-373.

[18] Li H, Zou J, Yao J, Peng H. The effect of TIG welding techniques on microstructure, properties and porosity of the welded joint of 2219 aluminum alloy. Journal of Alloys and Compounds. 2017; 727: 531-539.

[19] Milyardi I, Baskoro AS. Effect of current and speed on porosity in autogenous Tungsten Inert Gas (TIG) welding of aluminum alloys A1100 butt joint. In: IOP Conference Series: Materials Science and Engineering, International Conference on Materials Engineering and Applications, Bali, Indonesia; 14–16 January, 2018.